Smart Agricultural Technology 8 (2024) 100488

Contents lists available at ScienceDirect

Smart Agricultural Technology

journal homepage: www.journals.elsevier.com/smart-agricultural-technology

Speeding up UAV-based crop variability assessment through a data fusion approach using spatial interpolation for site-specific management

Sergio Vélez [a,b], Mar Ariza-Sentís [a,*], Marko Panić [c], Bojana Ivošević [c], Dimitrije Stefanović [c], Jere Kaivosoja [d], João Valente [a,e]

[a] Information Technology Group, Wageningen University & Research, 6708 PB Wageningen, Netherlands
[b] Group Agrivoltaics, Fraunhofer Institute for Solar Energy Systems ISE, 79110 Freiburg, Germany
[c] BioSense Institute, Center for Information Technologies, 21000 Novi Sad, Serbia
[d] Natural Resources Institute Finland (LUKE), Production Technologies, 00790 Helsinki, Finland
[e] Centre for Automation and Robotics (CAR), Spanish National Research Council (CSIC), 28006 Madrid, Spain

ARTICLE INFO

Keywords:
Spatial variability
TIN
IDW
Remote sensing
Satellite
Precision agriculture

ABSTRACT

Innovations in precision agriculture enhance complex tasks, reduce environmental impact, and increase food production and cost efficiency. One of the main challenges is ensuring rapid information availability for autonomous vehicles and standardizing processes across platforms to maximize interoperability. The lack of drone technology standardisation, communication barriers, high costs, and post-processing requirements sometimes hinder their widespread use in agriculture. This research introduces a standardized data fusion framework for creating real-time spatial variability maps using images from different Unmanned Aerial Vehicles (UAVs) for Site-Specific Crop Management (SSM). Two spatial interpolation methods were used (Inverse Distance Weight, IDW, and Triangulated Irregular Networks, TIN), selected for their computational efficiency and input flexibility. The proposed framework can use different UAV image sources and offers versatility, speed, and efficiency, consuming up to 98 % less time, energy, and computing requirements than standard photogrammetry techniques, providing rapid field information, allowing edge computing incorporation into the UAV data acquisition phase. Experiments conducted in Spain, Serbia, and Finland in 2022 under the H2020 FlexiGroBots project demonstrated a strong correlation between results from this method and those from standard photogrammetry techniques (up to $r = 0.93$). In addition, the correlation with Sentinel 2 satellite images was as strong as that obtained with photogrammetry-based orthomosaics (up to $r = 0.8$). The proposed approach could support irrigation leak detection, soil parameter estimation, weed management, and satellite integration for agriculture.

1. Introduction

Precision agriculture (PA) involves collecting and analyzing data from various sources, such as satellites or Unmanned Aerial Vehicles (UAVs, also known as drones), field sensors, and chemically analyzed soil samples to identify and manage field variability in a site-specific manner [1]. The Site-Specific Crop Management (SSM) approach is a type of PA that aims to improve resource application decision-making, such as water, fertilizers, pesticides, and agronomic practices, by better understanding the spatial variability of crop development factors [2]. Satellites, in combination with Geographic Information Systems (GIS), have long been used for remote sensing, with Vegetation Indices (VIs) as an effective way to analyze spatial variability in agriculture [3,4,5]. However, affordable sensors, which lower the cost barrier, have made advanced data collection techniques accessible to more farmers and agricultural professionals, increasing the importance of UAVs for remote sensing [6,7,8,9]. Nevertheless, in many cases, low to moderate-resolution images are sufficient to identify and map crop

Abbreviations: UAV, Unmanned Aerial Vehicles; SSM, Site-Specific Crop Management; PA, Precision Agriculture; GIS, Geographic Information Systems; VIs, Vegetation Indices; IDW, Inverse Distance Weight; TIN, Triangulated Irregular Networks; NGRDI, Normalized Green-Red Difference Index; GLI, Green Leaf Index; RGBVI, Red-Green-Blue Vegetation Index; VARI, Visible Atmospheric Resistance Index; RTK, Real Time Kinematics; LAI, Leaf Area Index; NDVI, Normalized Difference Vegetation Index; DO, Designation of Origin; CRS, Coordinate Reference System; WGS84, World Geodetic System 1984; EPSG, European Petroleum Survey Group; MSI, Multispectral Instrument; CRAN, Comprehensive R Archive Network.

* Corresponding author.
E-mail address: mar.arizasentis@wur.nl (M. Ariza-Sentís).

https://doi.org/10.1016/j.atech.2024.100488
Received 11 April 2024; Received in revised form 25 May 2024; Accepted 9 June 2024
Available online 14 June 2024

variability because it is often related to larger-scale factors such as soil type, topography, and management practices [10]. Hence, the choice of data source depends on the study's scope and research purpose, including the ground-level precision requirements and data capture frequency [11].

On the one hand, images at different scales and resolutions can provide similar results when analyzing patterns and spatial variability in heterogeneous agricultural fields [12,13] found strong correlations between satellite and UAV images despite severe differences in spatial resolution (10 × 10, 3 × 3, and 1 × 1 m per image pixel), reporting that satellite images were as effective as drone images in assessing general field conditions. [14] found that both UAV and Sentinel-2-derived NDVI (Normalized Difference Vegetation Index) values were effective in approximating LAI in maize fields, showing consistent trends. [15] observed that UAV-based data was more accurate than satellite data, but both were highly correlated and useful for creating detailed vineyard variability maps to improve grape yield and quality while minimizing costs and environmental impacts. Bollas et al. [16] found a high level of similarity between Sentinel 2 satellite imagery and UAV multispectral images, with both methods producing nearly identical average trends and a strong correlation. Moreover, in vertical trellis crops, as in continuous crops, Sentinel 2 and UAV imagery showed similar spatial variability trends and patterns of crop vigour [17]. Therefore, extensive detail is not always necessary to extract useful information from remotely sensed imagery.

On the other hand, UAVs have emerged as a valuable tool for

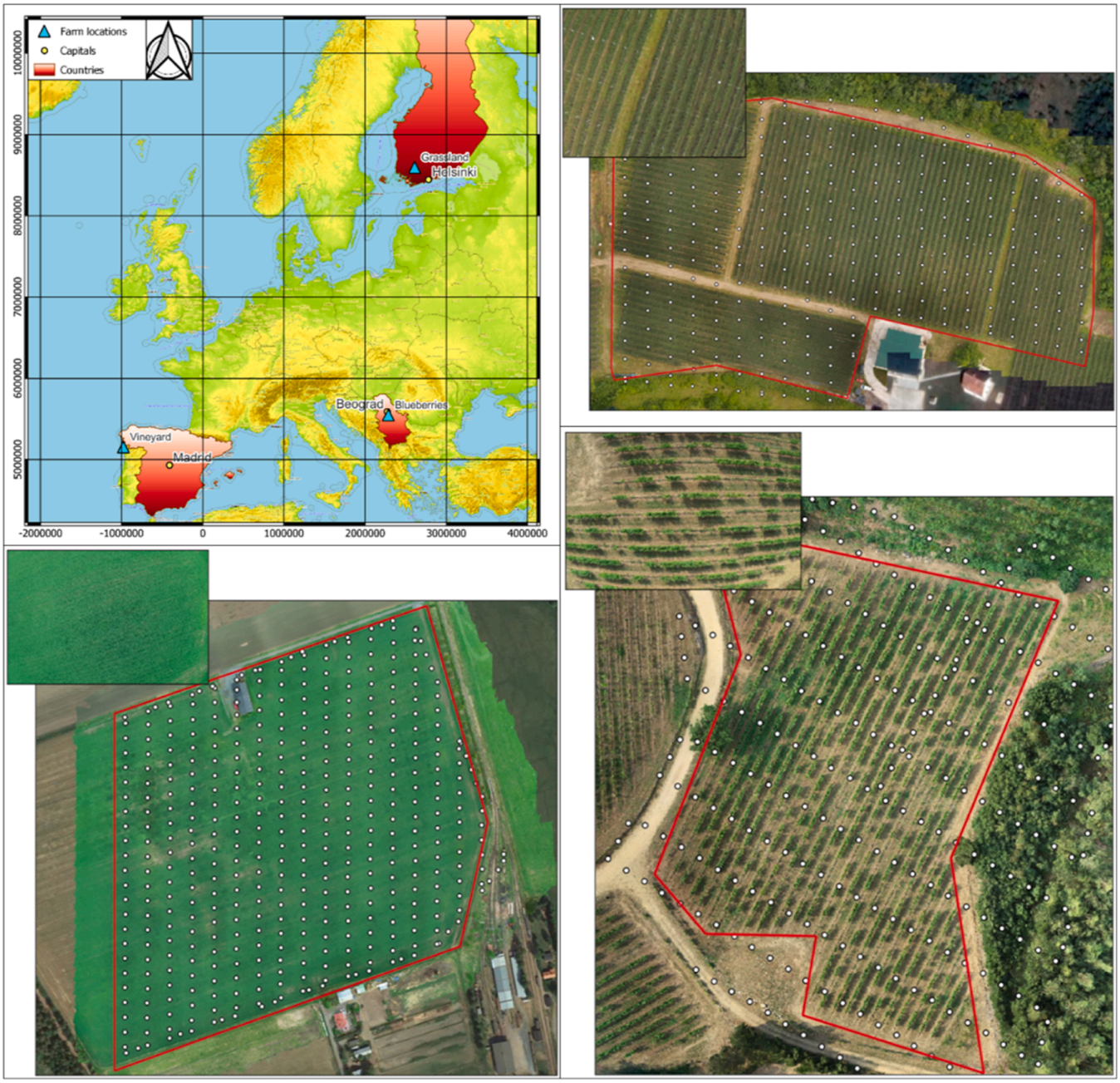

Fig. 1. Top-left: Location of agricultural plots. Vineyard: located in 'Tomiño, Pontevedra', Galicia, Spain (X: -979,061.0, Y: 5,154,269.1). Blueberries: located in Babe, Kosmaj, Serbia (X: 2,284,674.4, Y: 5,547,249.5). Grassland: located in Minkiö, Jokioinen, Kanta-Häme, Finland (X: 2,608,589.4, Y: 8,594,699.1). CRS WGS84 Pseudo-Mercator (EPSG: 3857**). Top-right:** Blueberry field. **Bottom-left:** Grassland. **Bottom-right:** Vineyard. Top-left: single image. Main: Orthomosaic. Red polygon: Region of Interest. White dots: position of the cameras during the flight.

generating VIs in agriculture, which help monitor crop growth, health, and productivity to optimize yield and improve overall efficiency [18]. UAVs offer advantages over satellite-based methods, such as higher resolutions. Nevertheless, satellite VIs have long yielded promising results, so combining their processing techniques with those of UAV VIs seems reasonable. Still, in agriculture, timely information can be as important as accurate data in certain situations because agricultural management decisions often require quick action to maximize yields and minimize losses. UAVs excel in this sense, facilitating timely information at critical phenological stages, allowing customized flights throughout the growing season [19,20]. This need will be even more significant in the coming years with the integration of robots in agriculture [21]. Additionally, these operations occur in remote environments, with restrictions such as equipment with reduced computing capacity or rural connectivity problems [22], which limits cloud-based information processing. In this scenario, although photogrammetric techniques are helpful in agriculture [9,23,24], they can require powerful computing resources and significant processing times.

Therefore, developing standardized multisource techniques, regardless of the platform and sensor used, is desirable to allow rapid assessment of agricultural variability using drone imagery. This research proposes a new UAV precision agriculture approach that addresses the challenges of i) standardization and interoperability between platforms and ii) fast processing of UAV data and real-time information.

2. Materials and methods

The experiments were part of the FlexiGroBots project and included three realistic scenarios implemented in commercial fields. These experiments were conducted in three locations across Europe: Spain, Serbia, and Finland (Fig. 1). Different crops were planted in each field: vineyards in Spain, blueberries in Serbia, and silage grasslands in Finland. Moreover, the UAVs and methodologies of image acquisition were different, resulting in various datasets composed of RGB and multispectral imagery (Table 1). All flights used RTK positioning with a 70–80 % overlap.

In Spain, UAV images were captured over a commercial vineyard, *Vitis vinifera* cv. Loureiro, located in Pontevedra, Galicia, Spain (X: -979,061.0, Y: 5,154,269.1; WGS84 Pseudo-Mercator, EPSG: 3857). Bodegas Terras Gauda, S.A., owns the vineyard, has an 8.1 % slope and 1.06 ha, and belongs to "Rias Baixas DO" (Designation of Origin). The grapevines, planted in 1990 with an NE-SW orientation, were trained using vertical shoot positioning (VSP). The distance between plants and rows is 2.5 and 3 m, respectively. The vineyard was managed in compliance with the DO protocol and legislation in force. Natural vegetation species grew as cover crops.

In Serbia, the images were taken over a commercial blueberry farm, *Vaccinium corymbosum* cv. Duke, located in Kosmaj mountain, village Babe, Serbia (X: -979,061.0, Y: 5,154,269.1; WGS84 Pseudo-Mercator, EPSG: 3857). The plantation is owned by Džodan Berry, with a slope of 2–3 % and covers 4 ha. Most plants were planted in 2015, with an expansion in 2018. The distance between plant rows is 3 m, with 1 meter between plants. Grass grows between rows, and the orchard complies with Global GAP food safety standards, other standards (SMETA, GRASP) and legislation in force.

In Finland, images were taken over a silage grassland managed by LUKE located in Jokioinen, Finland (X: 2,608,589.4, Y: 8,594,699.1; WGS84 Pseudo-Mercator, EPSG: 3857), with a mixture of grass varieties Timothy, Meadow fescue, and Clover and a relatively large occurrence of weeds (*Rumex longifolius*), forming an even canopy covering the soil almost completely. The grassland is about 16 ha and relatively even, with a 4-meter elevation difference.

2.1. Proposed framework

Photogrammetric techniques in agriculture use aerial imagery to gather data about crops and soil conditions, offering valuable insights but costly in terms of time and computational power. The efficiency and accuracy of these methods depend heavily on the image resolution and the overlap between aerial images [25]. Higher resolution leads to better quality but also increases costs, highlighting a trade-off between precision, computation power and time [26].

The proposed spatial variability map framework (Fig. 2) avoids photogrammetry. Instead, it uses UAV nadir images through parallel processing: a) extracting spectral data from a Region of Interest (ROI) to compute the VI, and b) extracting image metadata for geopositioning, and finally, combining spectral information with spatial points through data fusion. Finally, spatial interpolation generates the spatial variability map.

In order to validate the results, the spatial variability maps were compared to high-quality orthomosaics generated through standard photogrammetry processing.

The ROI dimensions are a function of the size of the image. In this study, the ROI was a square with sides starting at each image dimension's first and third quartiles (X and Y). The lower left vertex was the origin of coordinates (0,0) of the image, and Q_i was the quartile i relative to the maximum value in each dimension. The coordinates of the four vertices of the square are calculated as follows:

$$\text{Upper left vertex } A(x,y) = A(X_{Q1}, Y_{Q3}) = A(0.25 * X_{max}, 0.75 * Y_{max}) \quad (1)$$

$$\text{Upper right vertex } B(x,y) = B(X_{Q3}, Y_{Q3}) = B(0.75 * X_{max}, 0.75 * Y_{max}) \quad (2)$$

$$\text{Lower right vertex } C(x,y) = C(X_{Q3}, Y_{Q1}) = C(0.75 * X_{max}, 0.25 * Y_{max}) \quad (3)$$

$$\text{Lower left vertex } D(x,y) = D(X_{Q1}, Y_{Q1}) = D(0.25 * X_{max}, 0.25 * Y_{max}) \quad (4)$$

After defining the ROI, the image is cropped, and the different channels are extracted to calculate the VIs. The digital numbers were transformed into reflectance values following the procedure described in [27], although this procedure depends on the kind of sensor used. Four commonly used RGB-based VIs were employed in this study (Table 2): Normalized Green-Red Difference Index (NGRDI), Green Leaf Index (GLI), Red-Green-Blue Vegetation Index (RGBVI), and Visible Atmospheric Resistance Index (VARI). NGRDI is useful in determining optimal harvest times and predicting growth rates [28]. GLI enhances the identification of vegetated areas, critical for tasks requiring vegetated area masking or monitoring vegetation anomalies [29]. RGBVI

Table 1
Summary of UAV operations for Crop monitoring in different locations.

Country	Crop Type	UAV Model	Date/Time	Height	N.Images	Sensor Specifications	Area
Spain	Vineyard	DJI Phantom 4 RTK	12-Jul-22 18:31	30m	282	20-megapixel	1.06 ha
Finland	Grassland	DJI Phantom 4 RTK	01-Jun-22 11:06	60m	417	20-megapixel	16 ha
Serbia	Blueberries	DJI Phantom Multispectral	02-Jul-21 10:08	50m	309	Multispectral	4 ha

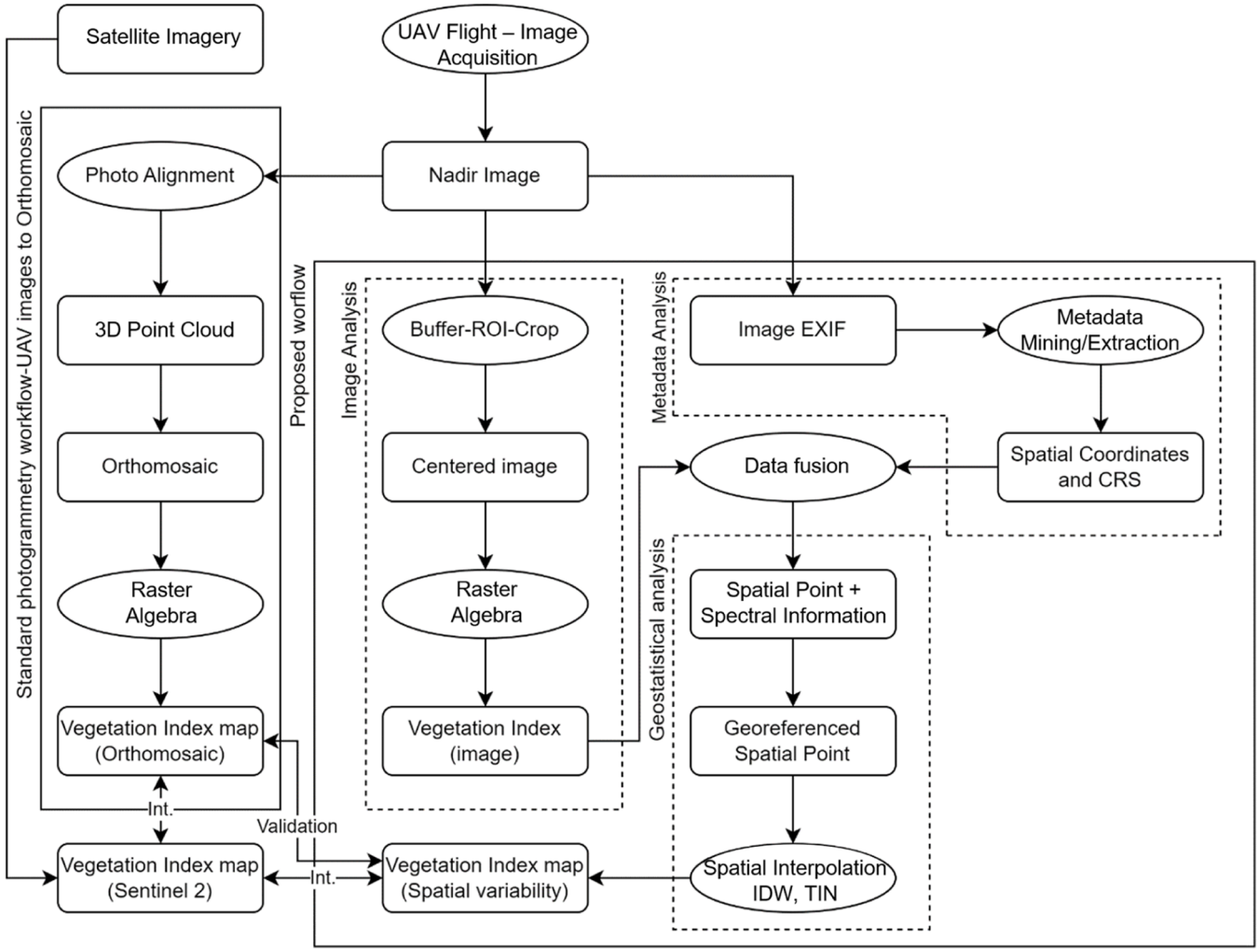

Fig. 2. Framework of the proposed methodology to obtain the spatial variability map through a data fusion approach. This methodology avoids photogrammetry by parallel processing of UAV nadir images and metadata, extracting spectral information and image positions. A data fusion process combines spatial points with spectral data, which are spatially interpolated to generate a spatial variability map. A standard photogrammetry workflow is used to validate the approach, and the results are compared to Sentinel 2 satellite imagery to assess integration possibilities.

Table 2
Vegetation indices. Wavelengths: Red, $\lambda = 640:760\ nm(\rho_{640:760})$. Green, $\lambda = 490:570\ nm(\rho_{490:570})$. Blue, $\lambda = 420:480\ nm(\rho_{420:480})$.

Vegetation Index	Equation	Reference
Normalized Green Red Difference Index	$NGRDI = \frac{(\rho_{490:570} - \rho_{640:760})}{(\rho_{490:570} + \rho_{640:760})}$	[32]
Green Leaf Index	$GLI = \frac{(2 * \rho_{490:570} - \rho_{640:760} - \rho_{420:480})}{(2 * \rho_{490:570} + \rho_{640:760} + \rho_{420:480})}$	[33]
Red-Green-Blue Vegetation Index	$RGBVI = \frac{(\rho^2_{490:570}) - (\rho_{640:760} * \rho_{420:480})}{(\rho^2_{490:570}) + (\rho_{640:760} * \rho_{420:480})}$	[30]
Visible Atmospherically Resistant Index	$\boldsymbol{VARI} = \frac{(\boldsymbol{\rho}_{490:570} - \boldsymbol{\rho}_{640:760})}{(\boldsymbol{\rho}_{490:570} + \boldsymbol{\rho}_{640:760} - \boldsymbol{\rho}_{420:480})}$	[34]

allows for early growth stage biomass prediction, essential for optimizing agricultural inputs and improving yield predictions [30]. Finally, VARI monitors crop growth in detail, helping in efficient field management and breeding programs [31].

Afterwards, spatial interpolation converts discrete observations into continuous data covering the field. Spatial interpolation estimates a variable's value at a specific location based on known values at other places [35]. Common methods are IDW, Inverse Distance Weight, and TIN, Triangulated Irregular Networks. In this study, IDW and TIN are chosen over other methods because of their suitability for regularly spaced data obtained from drone imagery. The IDW's simplicity and TIN's geometric adaptability are particularly advantageous for processing large datasets with a focus on speed and efficiency, ensuring minimal computational load.

IDW [36] assumes that nearby points are more similar than those farther away, using nearby values to estimate the value of a specific location and assuming that each measured location has a local impact that decreases as the distance between locations increases. The estimated value at a particular location is a weighted mean of nearby points:

$$\widehat{s}(x) = \frac{\sum_i^n w_i * s_i}{\sum_i^n w_i} \tag{5}$$

with

$$w_i = |x - x_i|^{-\beta},\ \beta \geq 0$$

where $\widehat{s}(x)$ is the estimated value at location x, s_i is the known value at location i, w_i is the weight assigned to the known value at location i based on its Euclidean distance x_i to the unknown location x. β is the

inverse distance power and represents the influence of a known point depending on the distance. As a result, higher weights are assigned to points closer to the unmeasured location, and the weight assigned to each point decreases as the distance increases [37]. IDW is fast to calculate, and it is flexible since β is equivalent to a bandwidth that smooths the results. Thus, in general, small values will generate smooth images, while high values will produce images similar to those from nearest-neighbor interpolation [38]. The default value is 2, as estimating β itself is challenging [37]. Aiming to automate the procedure, this work proposes an optimized β where the value is the Observed Mean Distance. An alternative method is TIN, which was first implemented in cartography in 1973 [39] and is widely used for terrain modelling, surface interpolation, and visualization applications. It is a vector data model that models a surface as contiguous, non-overlapping triangles whose vertices are the sampling points. The barycentric coordinates *(α, β, γ)* represent the relative distances of the unknown point from each triangle vertex [40], and their sum equals 1. Firstly, to interpolate the values of an unknown point $\hat{s}(x,y)$ within a triangle with known vertices $X(x_1,y_1)$, $Y(x_2,y_2)$, and $Z(x_3,y_3)$, the area of the triangle is calculated as:

$$A = \frac{1}{2}\left|x_1(y_2-y_3)+x_2(y_3-y_1)+x_3(y_1-y_2)\right| \quad (6)$$

These areas are calculated for each triangle within the system using the coordinates of the corresponding vertices and the unknown point. Subsequently, the barycentric coordinates can be computed as:

$$\alpha = \frac{A_1}{A}; \beta = \frac{A_2}{A}; \gamma = \frac{A_3}{A} \quad (7)$$

where A_1, A_2, A_3 are the areas of the triangles formed by the unknown point and each of the three vertices (*X, Y, Z*). Once the barycentric coordinates are determined, the value of the unknown point can be interpolated using the weighted sum of the values at the vertices of the triangle:

$$\hat{s}(x) = \alpha * p_x + \beta * p_y + \gamma * p_z \quad (8)$$

where p_x, p_y, p_z are the values at the vertices of the triangle. From the point of view of interpolation, it can be considered a local and exact method that calculates the information of any point on the surface by interpolating the vertices of the triangles that surround it, which form the vertices of the triangle containing the point [41].

2.2. Validation

Several orthomosaics for each location were generated to validate the generated spatial variability maps. To this end, a standard photogrammetric workflow was performed, using Agisoft Metashape Professional software, version 1.7.6 (Agisoft LLC, St. Petersburg, Russia), following the software's guidelines. The process involved optimizing camera positions and orientating data, generating a dense point cloud, and creating the orthomosaic. Photogrammetric reconstruction was conducted in low, medium, and high-quality settings to compare processing times. Furthermore, high-quality products served as validation for the maps generated by the proposed framework, calculating the same VIs for each process.

In the next step, three grids with varying tile sizes were used for the statistical analysis and comparison between each pair of UAV-based maps (Fig. 3). The first grid had a 1 m side to identify small-scale differences in the UAV maps, such as plant height and density variations. The second grid had a 3 m side to assess larger-scale differences, such as canopy cover. The third grid had a 10 m side, like Sentinel 2 imagery, to identify spatial variabilities, such as variations in irrigation, field topography, or management practices. This approach enabled comparing the UAV maps at different detail levels. Rectangular grids were used to balance tile size, bias and variability, with larger tiles reducing relative error but eliminating spatial variability within that area [38].

Finally, satellite images were downloaded for each location on the nearest cloud-free date to compare the results and evaluate their integration. Sentinel 2 products were chosen for their higher spatial resolution (10 m) and frequent revisit time (5 days) compared to other freely accessible satellite image sources. Thus, level 2A images captured by the MSI Instrument were downloaded: 8 July 2022 for Spain, 30 June 2021 for Serbia, and 30 May 2022 for Finland.

The computer used was a Linux 64-bit system (Ubuntu 20.04.4 LTS) with 64 GB RAM, Intel(R) Core(TM) i9–10940X CPU with 14 cores (28 threads) and a base frequency of 3.30 GHz (4.80 GHz in Turbo Boost Max mode). It had a Samsung SSD 860 EVO 1 TB and two Nvidia Titan RTX GPUs with a clock speed of 1770 MHz, 576 Tensor Cores, 4608 CUDA cores, and 24 GB GDDR6. Data analyses were conducted using QGIS (version 3.22.X, QGIS developer team 2022), and R software (version 4.2.X, R Foundation for Statistical Computing, R Core Team 2019, Vienna, Austria), including packages *raster, spatstat,* and *exifr*, from the Comprehensive R Archive Network (CRAN).

3. Results

For better clarity, statistical results for all fields are presented, but Fig. 4 highlights the VI generation process specifically for the vineyard, and Fig. 5 focuses on the NGRDI maps for each methodology and the three different crop fields across Europe.

Regarding the maps generated by each methodology (Fig. 5), similar patterns are observed in both orthomosaic-based maps and those based

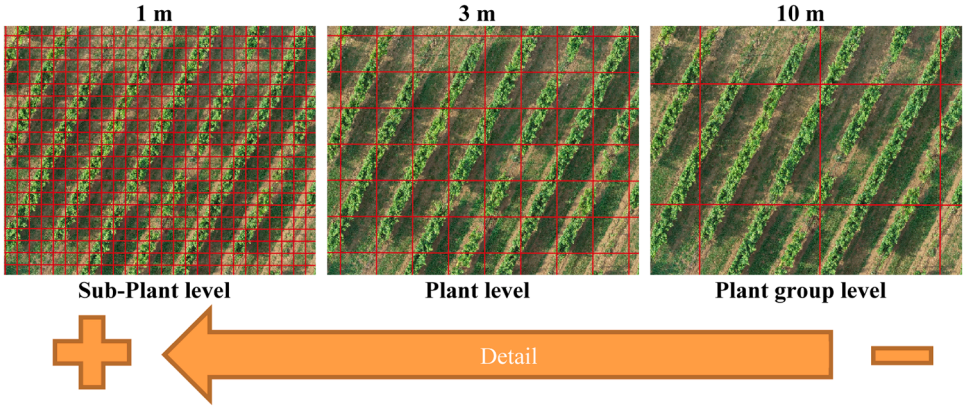

Fig. 3. Grid layers employed to analyze the spatial variability differences between the products. Three different grids with varying tile sizes were used. The first grid had a 1 m side, representing the sub-plant level; the second grid had a 3 m side, representing the plant level; and the third grid had a 10 m side, representing the plant-group level.

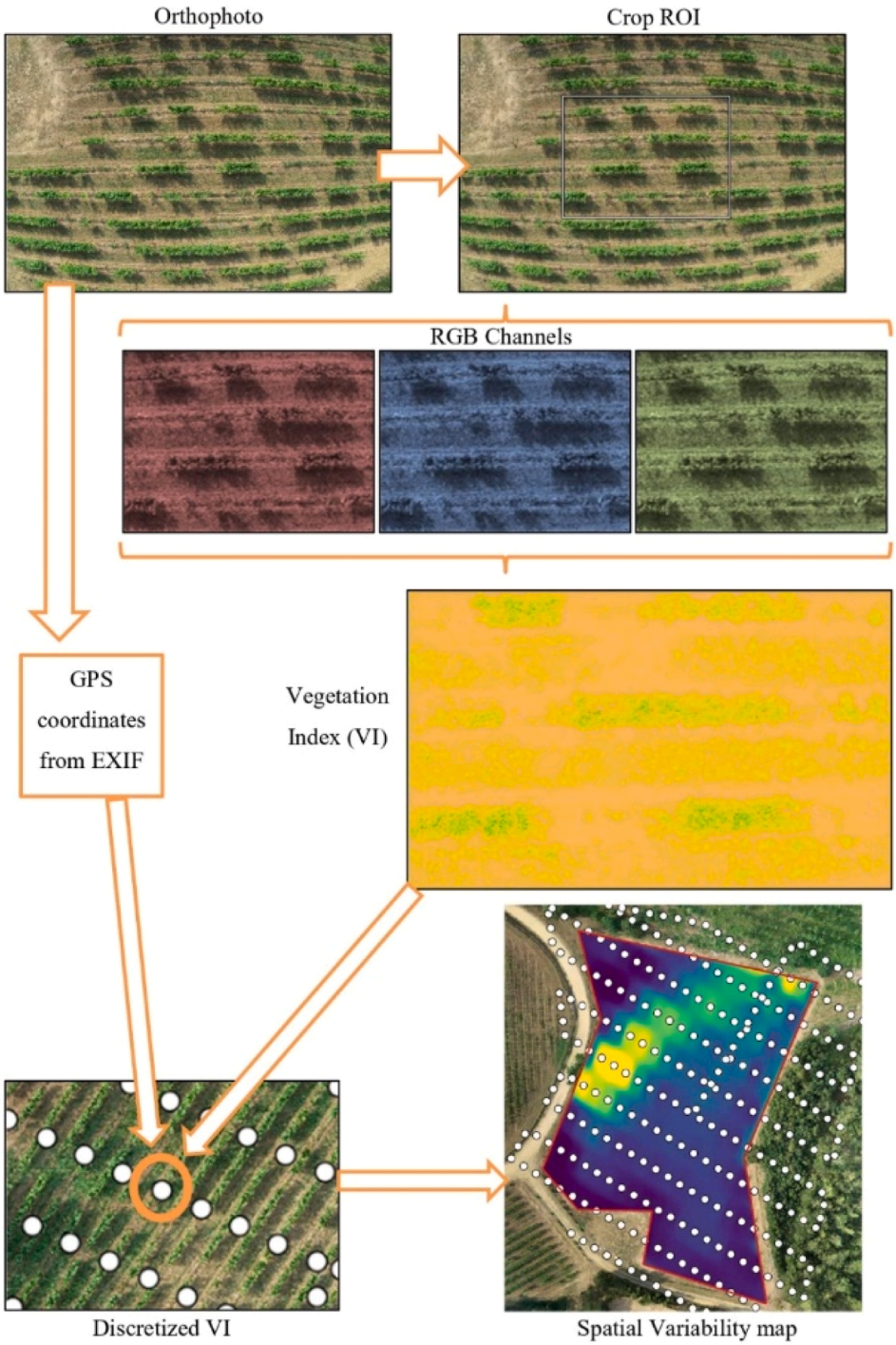

Fig. 4. Workflow including the generated product for the experiment in the vineyard. The initial inputs are the nadir images from the UAV flight. The Vegetation Index is calculated and discretized using the coordinates extracted from the metadata of each image. Finally, spatial interpolation is performed to generate the spatial variability map.

on IDW and TIN interpolation.

Thus, in the vineyard, higher VI values are found in the west, likely due to a tree shade. If observed in detail, a strip from the west to the northeast can be seen in both NGRDI maps, although less clear in the map calculated from the orthomosaic. For the blueberries, a path in the middle-west of the orthomosaic is clearly identifiable in the spatial variability maps, with several spots with spikes in VI, indicating higher vegetative development. In the grassland, two areas with low NGRDI are identified: one in the north, which is a shelter for agricultural machinery, and another in the west with poor vegetation density, visible even as bare soil in the orthomosaic.

For all sites, the maps generated by TIN are visually smoother than those by IDW, making it easier to identify regions with different VI values. However, a disadvantage of TIN compared to IDW is clear: in blueberries and grassland, TIN maps fail to interpolate values within the entire ROI, because TIN generation is limited to the vertices of the triangles. This issue does not arise in the vineyard case because the images were taken both inside and outside the ROI, making an optimum coverage.

Regarding IDW results, β values affect map quality (Fig. 6), with

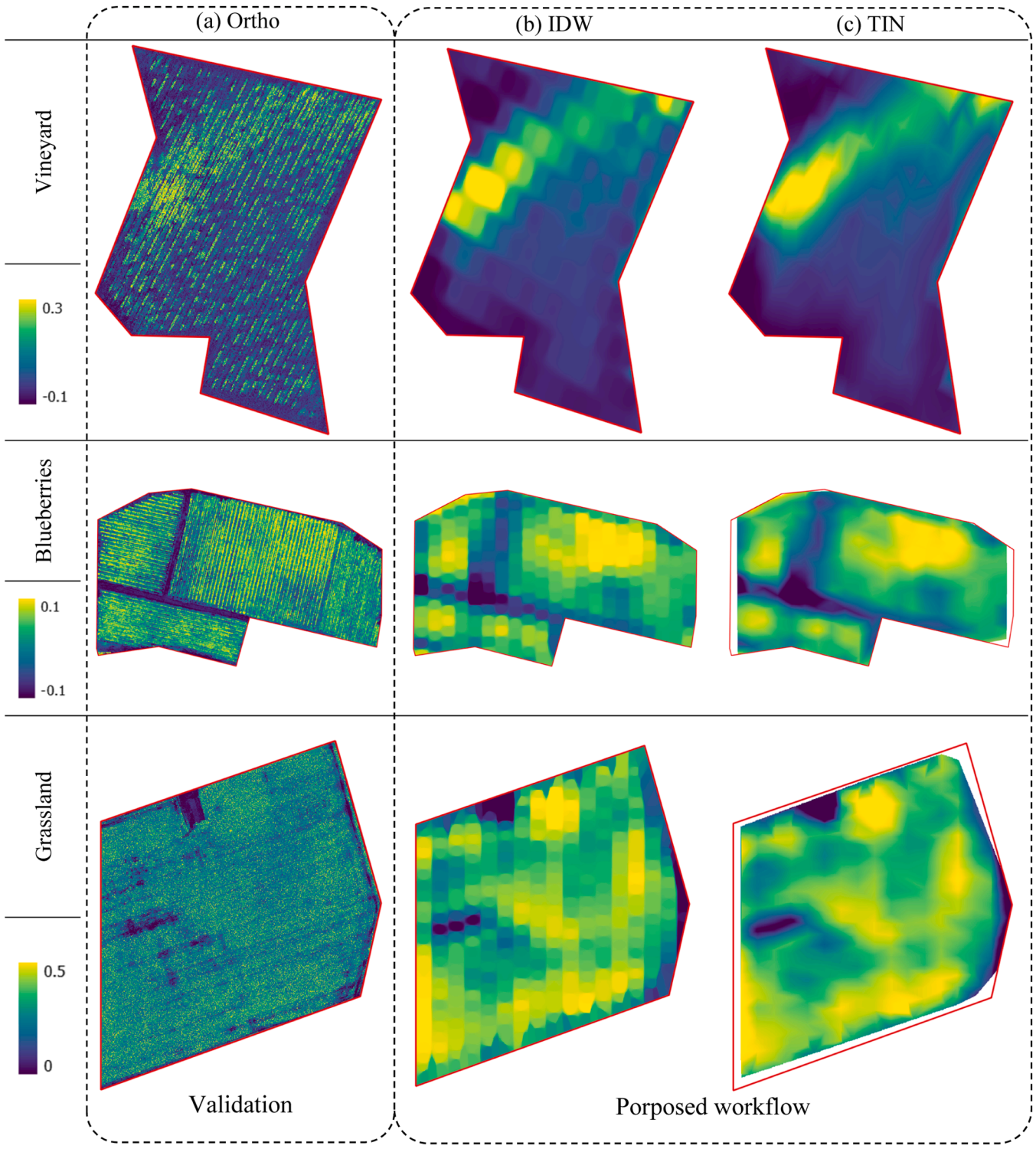

Fig. 5. Spatial variability maps based on Normalized Green-Red Difference Index (NGRDI) for each location generated using (a) orthomosaic, (b) optimized IDW, and (c) linear TIN for each field. The position of the cameras and the drone flight conditions were different in each field. WGS84 Pseudo-Mercator (EPSG: 3857).

lower values lacking interpolation and higher values showing highly differentiated zones. With $\beta = 2$, IDW produced maps with isolated information spots.

Spearman correlation analysis for the 10 m grid shows quite stable correlations regardless the VI used, with values reaching $r = 0.93$ for the vineyard (Fig. 7), $r = 0.93$ for the blueberries (Fig. 8), and $r = 0.86$ for the grassland (Fig. 9).

An initial exploratory analysis of the data (Fig. 7, Fig. 8, and Fig. 9) suggests lower spatial variability in the vineyard, likely due to its smaller size. Moreover, using simple regression, the best correlations appeared in the vineyard. The correlation values for IDW confirm that $\beta = 2$ had the worst correlations; therefore, it is not recommended. As anticipated, the correlations between the generated variability maps and the vegetation maps produced by the orthomosaics increase in all agricultural fields as the grid size increases, likely due to reduced spatial resolution, aligning the detail level of the orthomosaic with that of the spatial

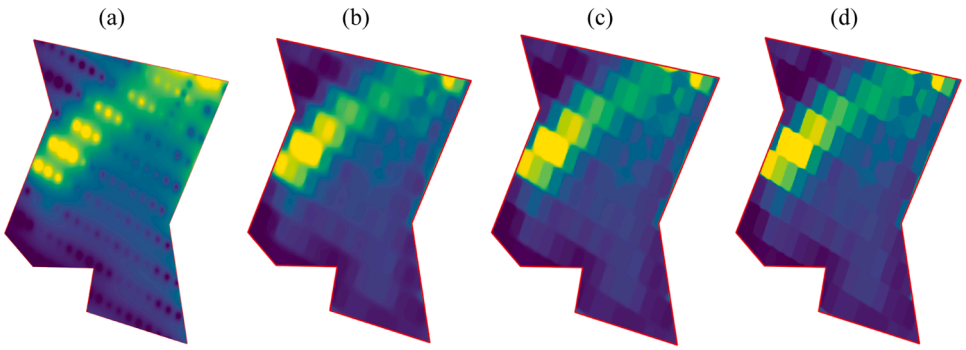

Fig. 6. Spatial variability maps of the vineyard based on Normalized Green-Red Difference Index (NGRDI) for each location generated using IDW and power of (a) β = 2, (b) the optimized value, β = 5, (c) β = 10, (d) β = 20. WGS84 Pseudo-Mercator (EPSG: 3857).

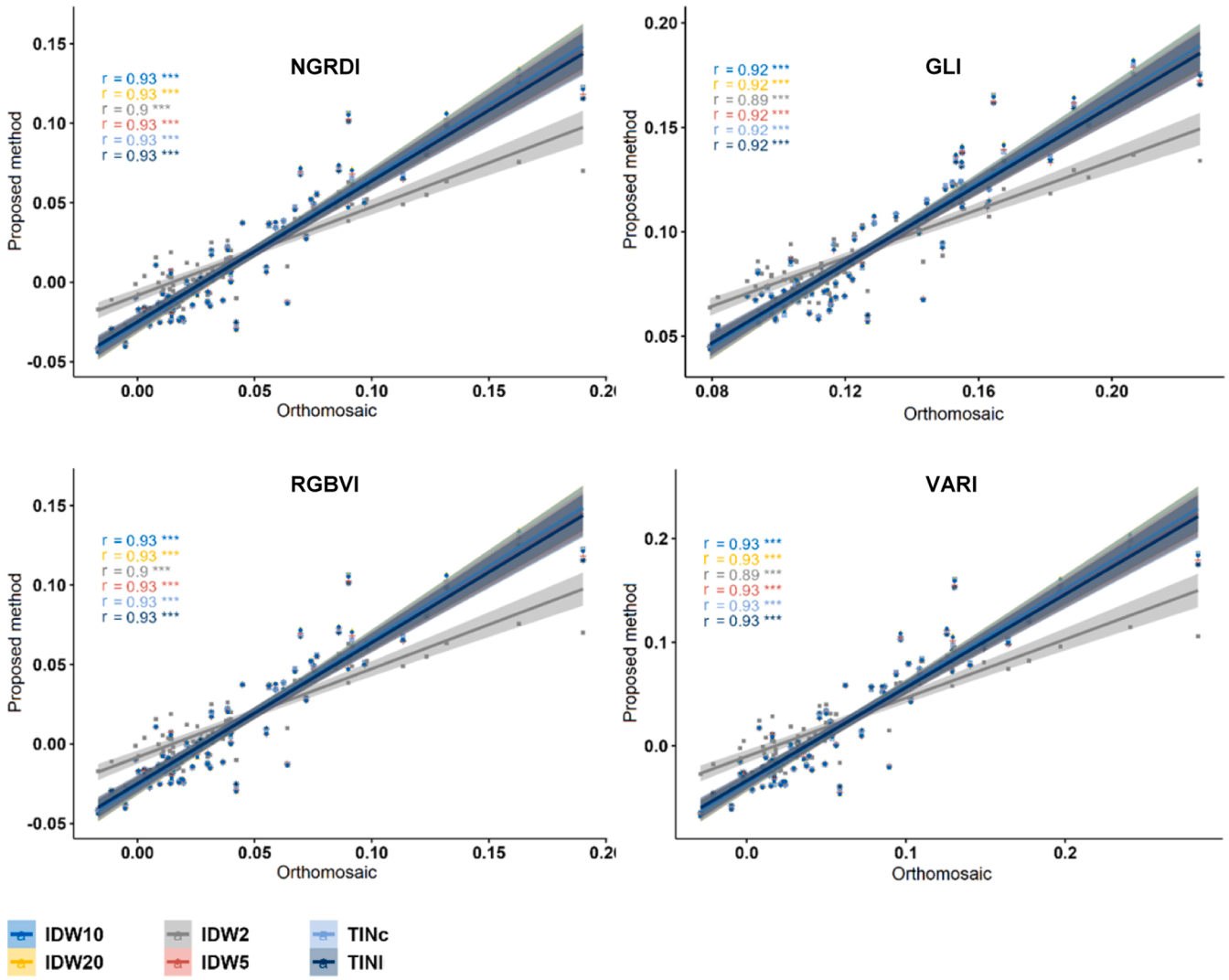

Fig. 7. Spearman correlation between the Vegetation Indices (NGRDI, GLI, RGBVI, and VARI) generated using the proposed methodology and a standard photogrammetric process in the vineyard. IDW10, Inverse Distance Weight, power of 10; TINl, Triangulated Irregular Networks (linear); TINc Triangulated Irregular Networks (cubic). Significance level: *p-value<0.05, **p-value<0.01, ***p-value<0.001.

variability maps.

TIN achieved better correlations than IDW in all cases, although they were very similar. TINc was slightly more correlated with orthomosaics than TINl, but the differences were minimal. Table 3 presents the correlations between the orthomosaic and TINc for each VI. As expected, correlation values gradually declined with 3 m and 1 m grids for statistical analysis, consistent with other research [42].

In addition, the correlations between products generated using UAV imagery and the Sentinel 2 images were also evaluated (Fig. 10). These images were compared to the vegetation maps derived from the orthomosaic and the maps generated using the proposed framework, specifically, TINl (TIN linear). Results showed similar values for both the

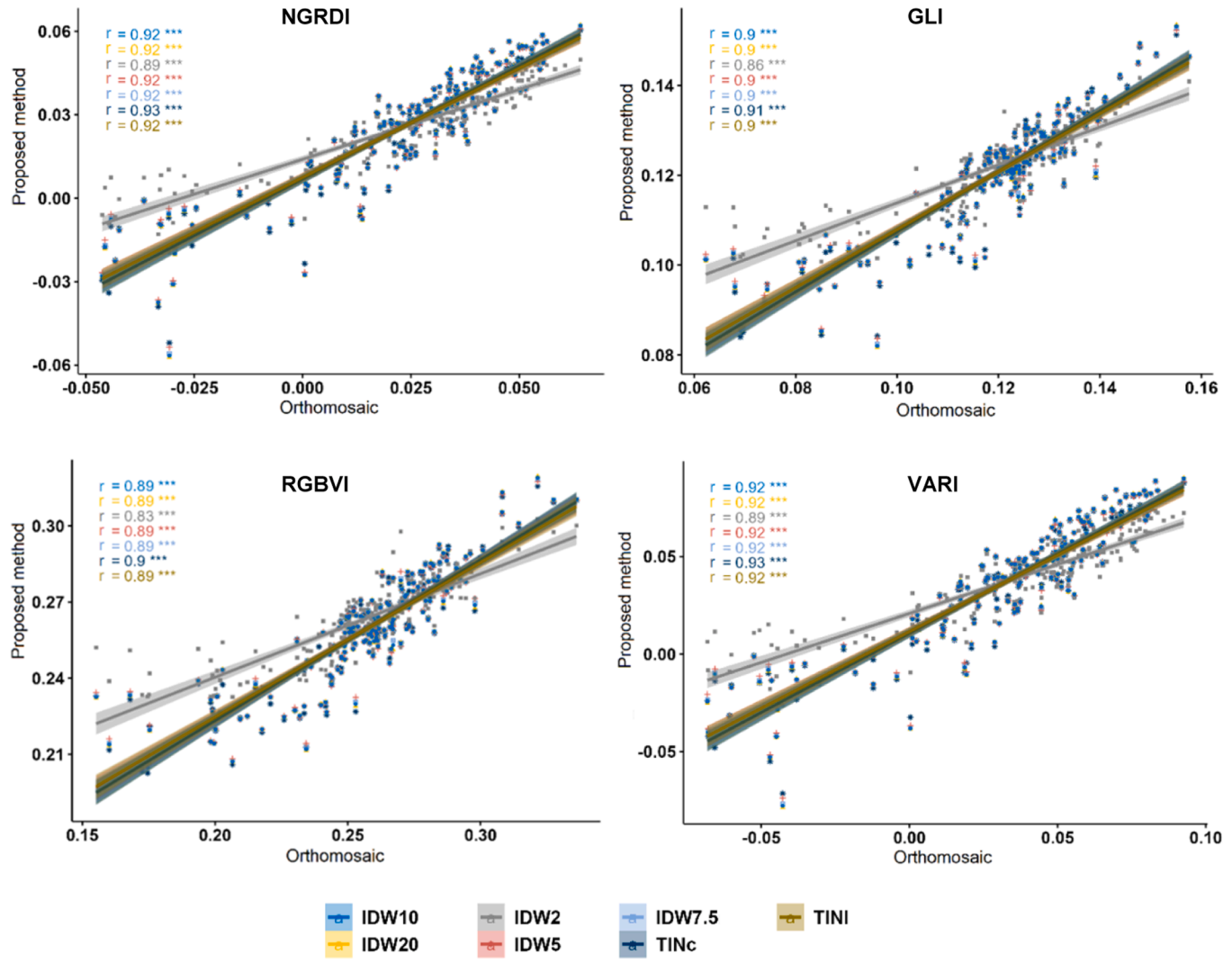

Fig. 8. Spearman correlation between the Vegetation Indices (NGRDI, GLI, RGBVI, and VARI) generated using the proposed methodology and a standard photogrammetric process in the blueberries. IDW10, Inverse Distance Weight, power of 10; TINl, Triangulated Irregular Networks (linear); TINc Triangulated Irregular Networks (cubic). Significance level: *p-value<0.05, **p-value<0.01, ***p-value<0.001.

orthomosaic-derived maps and those generated using the proposed framework.

Finally, processing times were analyzed (Fig. 11). This information is critical when working with robots in agricultural fields, where device communications and connectivity may be limited and have low bandwidth. It is worth recalling that the number of images differed for each field (vineyard, 282 images; blueberries, 309 images; grassland, 417 images).

All interpolation methods were efficient and very fast, with TIN more efficient than IDW, taking up to 93 % less time in the grassland. Within TIN, the linear method was quicker than the cubic. The proposed methodology was almost 88 % faster on average compared to the low-quality photogrammetric flow, and up to 97 % faster than the high-quality photogrammetric process. Specifically, the proposed data fusion approach required 94 % less time in the vineyard, 78 % less in grassland, and 92 % less in blueberries compared to the low-quality photogrammetric process, and 98 %, 94 %, and 98 % less time, respectively, when compared to the high-quality process.

4. Discussion

This research used several low-cost UAVs in real scenarios to generate four commonly used RGB VIs. When comparing VIs, it is essential to consider their suitability for specific applications. For example, the NGRDI index, used as the guiding thread of this work, has proved to help evaluate nitrogen balance in wheat [43]; still, it struggles with vegetation identification in complex backgrounds [44]. No such issues occurred in this research, with VI maps showing similar spatial variability patterns. Moreover, this research develops a real-time image processing methodology to use images efficiently, making the choice VI irrelevant, allowing the calculation of other VIs, such as the better-known NDVI. Thus, geopositioning enables this framework to be fully compatible with any image, such as RGB and multispectral. This characteristic expands the framework capabilities since multispectral image-based VIs are particularly useful for agricultural tasks like estimating the risk of fungal disease in vineyards [45,46] and identifying crop growth trends and health [47,48,49].

Similarly, in this research, these VI spatial variability maps can be helpful for quick assessment of potential issues: in Finland, for example, for quickly mapping the vegetation daily and highlighting areas with lower plant development. In Spain, the belt observed in the IDW and TIN maps (Fig. 5) is a common agricultural spatial phenomenon that could be related to factors like topography and ephemeral streams [50], and the differences in altitude resulting in a northern depression can cause water and sediment transport, altering soil texture and composition, affecting plant development and resulting in spatial variability [51]. In

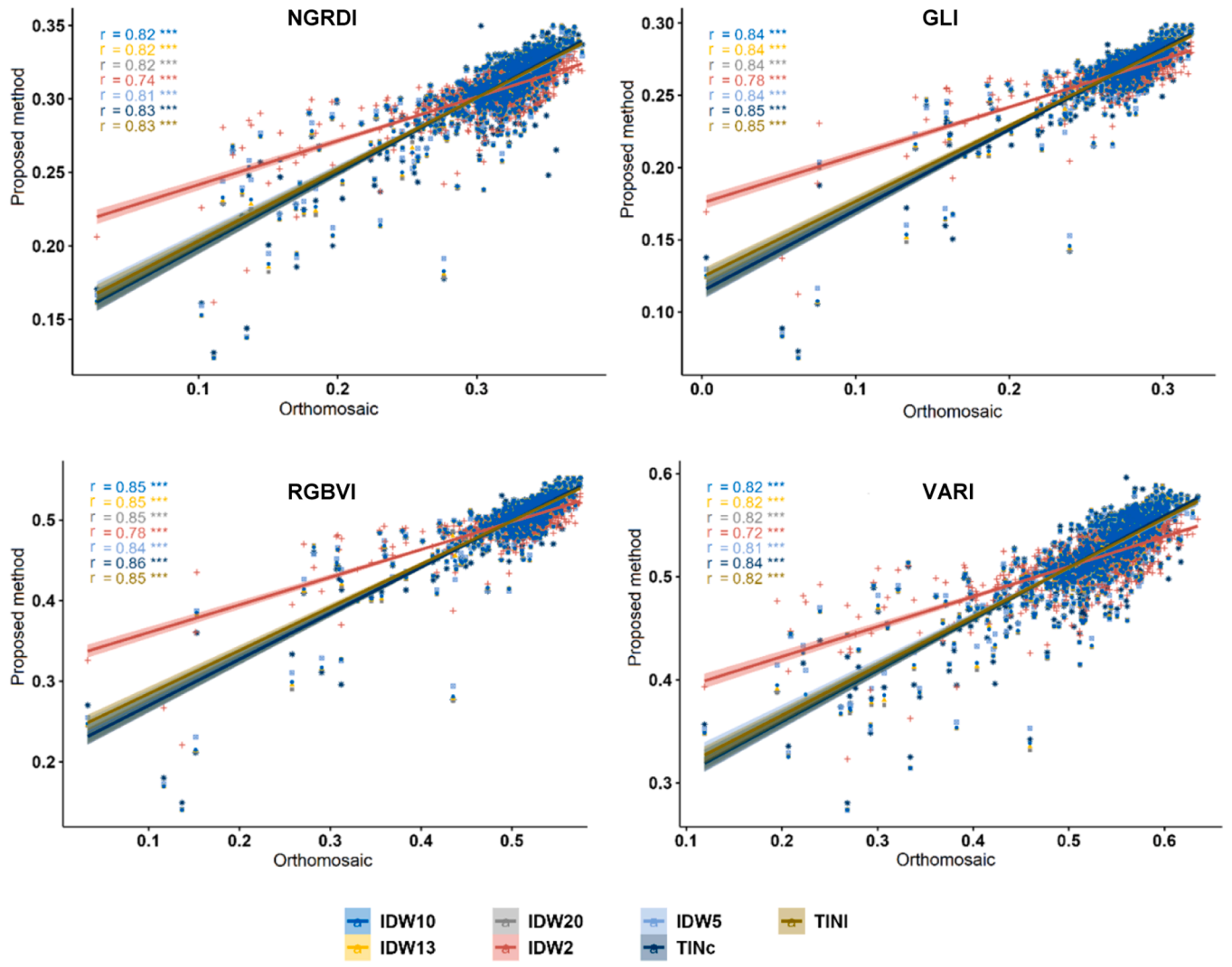

Fig. 9. Spearman correlation between the Vegetation Indices (NGRDI, GLI, RGBVI, and VARI) generated using the proposed methodology and a standard photogrammetric process in the grassland. IDW10, Inverse Distance Weight, power of 10; TINl, Triangulated Irregular Networks (linear); TINc Triangulated Irregular Networks (cubic). Significance level: *p-value<0.05, **p-value<0.01, ***p-value<0.001.

Table 3
Spearman correlation between the orthomosaic and TINc for the 1 m and 3 m grids and each Vegetation Index. NGRDI, Normalized Green Red Difference Index; GLI, Green Leaf Index; RGBVI, Red-Green-Blue Vegetation Index and; VARI Visible Atmospherically Resistant Index. All values had a p-value<0.001.

Vegetation Index	Tile size					
	1 m			3 m		
	Vineyard	Blueberries	Grassland	Vineyard	Blueberries	Grassland
NGRDI	0.52	0.58	0.60	0.71	0.74	0.67
GLI	0.44	0.46	0.65	0.64	0.65	0.71
RGBVI	0.42	0.41	0.66	0.63	0.60	0.72
VARI	0.54	0.58	0.60	0.72	0.74	0.67

addition, ephemeral streams can cause small gullies, making characteristic spatial patterns within the field that influence plant development [52]. Other factors, such as crop management operations, can reduce the natural variability caused by soil and topography [53]. Hence, despite the lower resolution, the maps generated using the proposed approach effectively capture spatial variability, and the adaptable input requirements (multiple sensors and geostatistical interpolation, reducing computational demands for rapid assessments) makes this framework versatile and suitable for many purposes.

Depending on the field, the proposed framework demonstrated a speed improvement up to 98 % faster and, on average, 88 % faster than methods based on photogrammetry. This speed is crucial as technology becomes more prevalent in agriculture. Additionally, it is particularly important for many farms that cannot invest in the latest, most expensive equipment, and even when they can, they often face challenges due to image processing difficulties caused by hardware constraints and computational limitations [54]. The experiment's outcomes are highly reliable as they were conducted in three locations across Europe: Spain, Serbia, and Finland (Fig. 1), involving diverse UAVs and sensors, various crop types, and various weather conditions. Similar findings by other

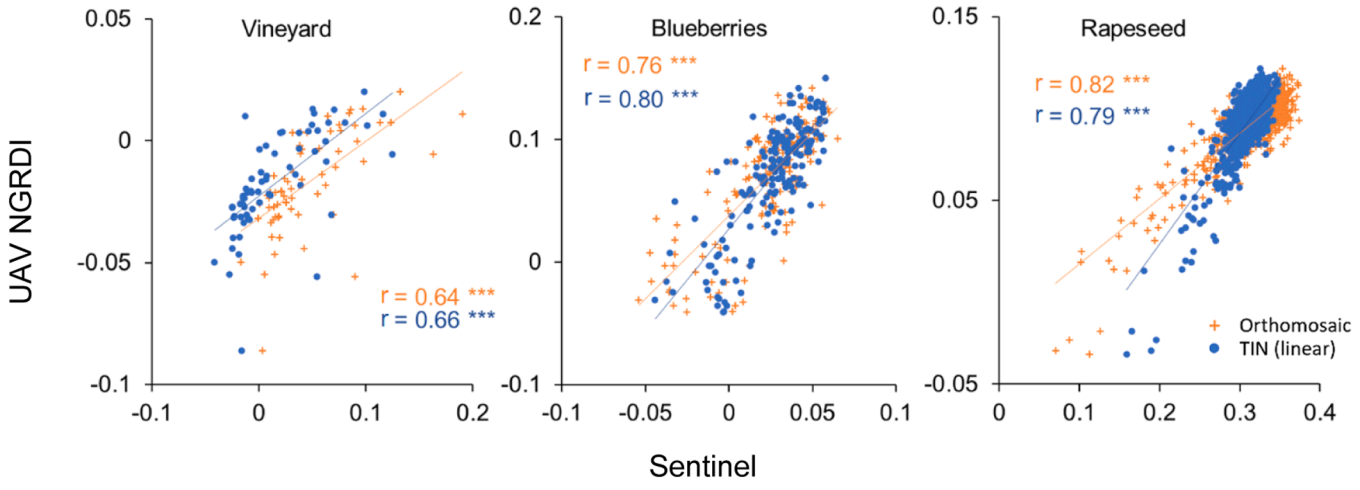

Fig. 10. Relationship between Sentinel 2 imagery and the UAV Vegetation Indices (NGRDI) generated using the Orthomosaic and the proposed methodology (TIN linear). Significance level: *p-value<0.05, **p-value<0.01, ***p-value<0.001.

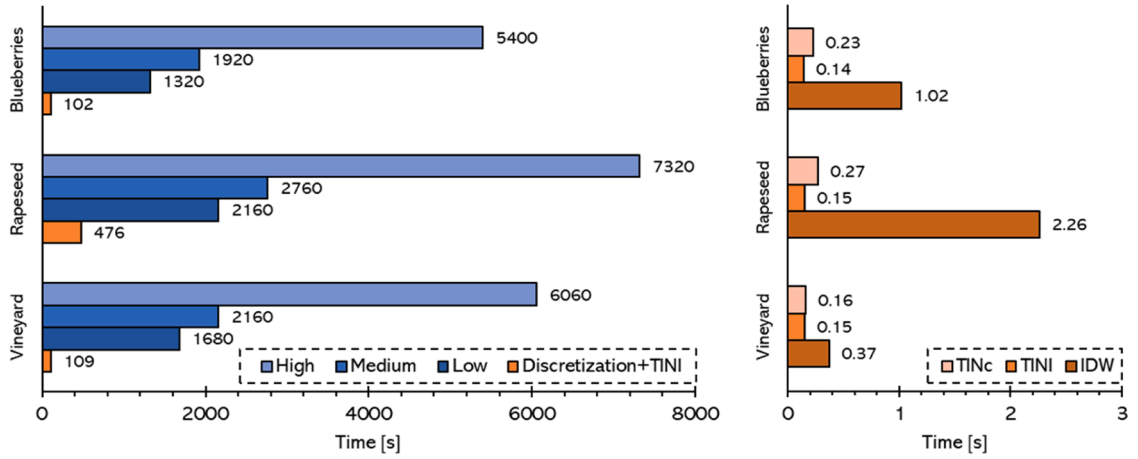

Fig. 11. Time required for each process (values in seconds). Standard Photogrammetry process in Low, Medium, and High quality. The proposed methodology shows the times required for discretization (images to points) and interpolations: IDW, Inverse Distance Weight; TINl, Triangulated Irregular Networks (linear); TINc, Triangulated Irregular Networks (cubic).

authors using different resolutions indicate that while lower-resolution images provide less detail, they are fair enough to assess vegetation trends and spatial variability [12,13,15–17,55] suggested that if the objective is not to screen each vine individually, lower-resolution images might enhance efficiency in mapping vine yield or spatial variations, leading to stronger correlations.

The proposed methodology provided insights into the spatial variability in hedgerow crops, such as vineyards and blueberries, as vegetation changes directly correlate with the spectral sensor data, even in non-continuous crops [17,56] found comparable results, where missing plants and bare soil minimally affected spectral and agronomical information. The findings related to spatial interpolation revealed that IDW power β significantly affected the map accuracy. The default value (β =2) is not advisable because it generated non-continuous maps and consistently showed lower correlations. Conversely, very high values only considered the immediately surrounding points for the estimation, creating completely different zones with sharp edges. It is worth considering that agricultural phenomena are frequently continuous, but specific events like weed patches or irrigation leaks can occur, so high power values can create maps that hide these phenomena. This distance should cover UAV image locations to avoid gaps and be calibrated based on the inputs. The proposed technique for automatic power estimation may be handy in automating the process. In addition, IDW is a precise interpolation method, with the highest and lowest values at sample points [37], making it sensitive to outliers and clustering. However, UAV images collected in adequate missions rarely have outliers, and any would be easily detectable before the interpolation process.

TIN interpolation proved more efficient than IDW despite some problems at the field boundaries. It systematically required less time in all agricultural plots, with up to 93 % less time in the grassland. These results align with other studies recommending TIN over IDW for topographic map generation [57]. TIN is also valid for creating digital elevation models to predict wetland vegetation communities from LiDAR data points [58]. Additionally, the TIN linear method was faster than the cubic method due to its simpler mathematical operations. Unlike the cubic method, which calculates the spline between points, the linear method directly connects these points with straight lines, avoiding the need for solving cubic equations for each interpolated point and significantly reducing the complexity of calculations, especially in datasets with a large number of points, as is common in UAV-derived agricultural data.

Therefore, the proposed framework is efficient and provides reasonable results compared to those derived from more computationally demanding techniques. While this approach may not be ideal for situations requiring high precision or complex scenarios with small

vegetation gradients [12], it is advantageous when spatial variability has to be assessed quickly with lower resolution requirements.

4.1. Advantages, limitations, and challenges

The proposed methodology, like any methodology based on remote sensing techniques, has some potential advantages and limitations:

- At the outset, VIs are calculated on individual images at the network's edge, using only the necessary information to create spatial variability maps. This reduces file size, which is advantageous in low-bandwidth scenarios and robot fleet interconnections. Agricultural fields, typically located in rural areas, face different constraints than urban areas, such as connectivity issues or isolation, which are critical for adopting new technologies [59].
- The proposed methodology, requiring only geotagged images captured by any sensor, can be integrated into more complex processes. For example, to provide inputs for disease mapping based on spatial variability analysis [46], improving real-time results without complex computational techniques like photogrammetry.
- Lower resolution can be problematic in crops with mixed pixels, a well-known issue in satellite imagery. This issue is less significant in crops that cover the entire surface but is notable in hedgerow crops [56]. Despite this, the vineyard and blueberries did not perform worse than the grassland in this research.
- Accurate georeferencing is crucial since geostatistical interrelation depends on precise image coordinates. With the Real Time Kinematics (RTK) positioning systems used in this research, accuracy issues should be minimal.
- The effectiveness of this methodology depends on UAV mission coverage because the VI values are fused with image geodata. However, this issue is similar to techniques such as photogrammetry, requiring sufficient overlap [60]. In contrast, using geostatistical algorithms, the proposed data fusion approach will always generate continuous maps. However, maps' reliability is affected by the modifiable areal unit problem (MAUP), which is inherent to any spatially aggregated data study [61]. MAUP reflects the true nature of natural systems with hierarchical structures, aiding in understanding spatial phenomena and dynamics of complex natural systems [62], such as agricultural systems.
- The proposed method is scalable across various crops and climates, proven in tests in Spain, Serbia, and Finland with different missions, UAVs, sensors, and crops. Its flexibility with VIs and compatibility with RGB and multispectral imagery ensure it can be applied effectively in many agricultural scenarios.

Alternatively, the proposed approach could support agricultural operations such as:

- Quickly assessing irrigation leaks. UAV visible imagery can contribute to evaluating soil moisture levels [63]. Irrigation leaks can lead to problems such as mud puddles, a hazard to UGVs (unmanned ground robots) and human-operated vehicles, such as cars or tractors, potentially compromising occupants. Early detection of these leaks could improve operational efficiency and safety.
- Estimating soil parameters during bare soil periods [64,65]. The visible electromagnetic spectrum can provide insights into soil organic carbon content [66].
- Providing real-time or near real-time information. The spatial variability maps show different field areas at a glance (Fig. 5), which can be very handy for technicians. Fast information transfer to other robots is essential in the context of robot fleets and Edge Computing scenarios and allows for quick perception, decision-making, and action.
- Establishing site-specific weed management zones, a cost-effective and eco-friendly strategy supporting the EU-Green Deal, and promoting biodiversity while reducing pesticide usage in agriculture [67] without negatively affecting crop yields or incurring additional weed management expenses.
- Integration with satellite Remote Sensing. UAV data can align with satellite data by upscaling UAV imagery to satellite-level resolution, enhancing satellite-based vegetation monitoring [42]. The proposed framework can fill gaps in satellite time series and could be particularly interesting in cloud-prone areas like the Finish grassland.

Future research could refine this framework for better spatial variability detection. Potential improvements may include canopy-focused vegetation segmentation, two-dimensional LAI calculations using the shadows method [68], and exploring other spatial interpolation techniques to enhance map accuracy [69]. Still, considering the time spent in each process (Fig. 11), the bottleneck is in the data fusion step (image discretization and VI generation at the spatial point), so reducing computing time with filters or other techniques before VI generation could be beneficial. Partitioning information to generate maps progressively could be another improvement, as spatial interpolation uses n points, mainly when TIN is used. Finally, integrating deep learning for image preprocessing could offer promising advancements in plant classification despite challenges such as generalizability, interpretability, time and computational cost, and high training demands [70,71]. Nevertheless, enhancements should always focus on delivering quick information for real-time operations.

5. Conclusions

This research highlights UAV-based methods for rapid, cost-effective data collection in precision agriculture. Using geotagged images enables real-time monitoring for timely crop management decisions. This framework uses data fusion and geostatistical interpolation methods (IDW and TIN) to generate spatial variability maps from any set of geotagged nadir images. These maps, derived from spectral information and EXIF metadata, correlate highly with photogrammetry-based maps (up to $r = 0.93$) but are faster to generate and less computationally expensive. Therefore, they are more sustainable in terms of energy. TIN was the most efficient technique within the proposed framework, correlating well with Sentinel 2 imagery (up to $r = 0.8$), similar to the correlation level with the maps derived from the orthomosaic.

The method offers accurate and reliable spatial information critical for constructing spatial variability maps for Site-Specific Crop Management (SSM). This standardised framework has two key advantages: i) interoperability and versatility, since any nadir image can be used as input, with no training or previous knowledge of the field required, and ii) speed and efficiency, consuming up to 98 % less time (and therefore, energy).

The maps generated using this methodology are as effective as those produced through photogrammetry for spatial variability analysis purposes but consume up to 98 % less time, energy and computing requirements than standard photogrammetry techniques. This adaptable, cost-effective framework enhances site-specific crop management by quickly identifying spatial variability and optimizing practices. It also supports immediate field information and potential for multiscale remote sensing, including satellite integration, but requires fewer computer resources with efficient processing and transmission in low-bandwidth scenarios, such as those in rural areas. Future research should refine the proposed framework, incorporating techniques like canopy-focused vegetation segmentation. Additionally, optimizing computing time through two-dimensional LAI calculations and advanced filters for image preprocessing could significantly improve real-time operational efficiency.

Ethics approval and consent to participate

Not applicable.

Consent for publication

Not applicable.

CRediT authorship contribution statement

Sergio Vélez: Conceptualization, Methodology, Software, Validation, Formal analysis, Investigation, Resources, Data curation, Writing – original draft, Writing – review & editing, Visualization, Supervision, Project administration, Funding acquisition. **Mar Ariza-Sentís:** Software, Formal analysis, Investigation, Resources, Data curation, Writing – review & editing, Visualization. **Marko Panić:** Resources, Data curation, Writing – review & editing, Project administration, Funding acquisition. **Bojana Ivošević:** Resources, Data curation, Writing – review & editing. **Dimitrije Stefanović:** Resources, Data curation, Writing – review & editing. **Jere Kaivosoja:** Resources, Data curation, Writing – review & editing, Project administration, Funding acquisition. **João Valente:** Validation, Resources, Data curation, Writing – review & editing, Supervision, Project administration, Funding acquisition.

Declaration of competing interest

The authors declare that they have no known competing financial interests or personal relationships that could have appeared to influence the work reported in this paper.

Data Availability

Data will be made available on request.

Acknowledgements

This work has been carried out in the scope of the H2020 Flexi-GroBots project, which the European Commission has funded in the scope of its H2020 program (contract number 101017111, https://flexigrobots-h2020.eu/). Dr. Sergio Vélez's postdoctoral fellowship contract has been supported by the Iberdrola Foundation and the European Commission under the Marie Skłodowska-Curie Actions (MSCA)—E4F, part of the Horizon 2020 program (Grant Agreement No 101034297, https://doi.org/10.3030/101034297). The authors acknowledge valuable help and contributions from 'Bodegas Terras Gauda, S.A.' and all project partners.

References

[1] R. Gebbers, V.I. Adamchuk, Precision agriculture and food security, Science 327 (5967) (2010) 828–831, https://doi.org/10.1126/science.1183899.
[2] P. Zarco-Tejada, N. Hubbard, P. Loudjani, Precision agriculture: an opportunity for EU farmers – potential support with the CAP 2014–2020, *Joint Res. Centre (JRC) of the Eur. Comm. Monitor. Agric. ResourceS (MARS), Unit H04, Brussels, Belgium* 56 (2014).
[3] E. Barajas, S. Álvarez, E. Fernández, S. Vélez, J.A. Rubio, H. Martín, Sentinel-2 satellite imagery for agronomic and quality variability assessment of pistachio (Pistacia vera L.), Sustainability 12 (20) (2020) 8437, https://doi.org/10.3390/su12208437.
[4] D. Helman, I. Bahat, Y. Netzer, A. Ben-Gal, V. Alchanatis, A. Peeters, Y. Cohen, Using time series of high-resolution planet satellite images to monitor grapevine stem water potential in commercial vineyards, Remote. Sens. 10 (10) (2018) 1615, https://doi.org/10.3390/rs10101615.
[5] M. Sozzi, A. Kayad, S. Gobbo, A. Cogato, L. Sartori, F. Marinello, Economic comparison of satellite, plane and UAV-Acquired NDVI images for site-specific nitrogen application: observations from Italy, Agronomy 11 (11) (2021) 2098, https://doi.org/10.3390/agronomy11112098.
[6] F. Ahmed, J.C. Mohanta, A. Keshari, P.S. Yadav, Recent advances in unmanned aerial vehicles: a review, Arabian J. Sci. Eng. 47 (7) (2022) 7963–7984, https://doi.org/10.1007/s13369-022-06738-0.
[7] M. Ariza-Sentís, J. Valente, L. Kooistra, H. Kramer, S. Mücher, Estimation of spinach (Spinacia oleracea) seed yield with 2D UAV data and deep learning, Smart Agric. Technol. 3 (2023) 100129, https://doi.org/10.1016/j.atech.2022.100129.
[8] D.-W. Kim, S.J. Jeong, W.S. Lee, H. Yun, Y.S. Chung, Y.-S. Kwon, H.-J. Kim, Growth monitoring of field-grown onion and garlic by CIE L*a*b* color space and region-based crop segmentation of UAV RGB images, Precision Agric. (2023), https://doi.org/10.1007/s11119-023-10026-8.
[9] S. Vélez, R. Vacas, H. Martín, D. Ruano-Rosa, S. Álvarez, A novel technique using planar area and ground shadows calculated from UAV RGB imagery to estimate pistachio tree (Pistacia vera L.) canopy volume, Remote. Sens. 14 (23) (2022) 6006, https://doi.org/10.3390/rs14236006.
[10] J.W. Hansen, J.W. Jones, Scaling-up crop models for climate variability applications, Agric. Syst. 65 (1) (2000) 43–72, https://doi.org/10.1016/S0308-521X(00)00025-1.
[11] E. Alvarez-Vanhard, T. Corpetti, T. Houet, UAV & satellite synergies for optical remote sensing applications: a literature review, Sci. Remote Sens. 3 (2021) 100019, https://doi.org/10.1016/j.srs.2021.100019.
[12] A. Matese, P. Toscano, S. Di Gennaro, L. Genesio, F. Vaccari, J. Primicerio, C. Belli, A. Zaldei, R. Bianconi, B. Gioli, Intercomparison of UAV, aircraft and satellite remote sensing platforms for precision viticulture, Remote. Sens. 7 (3) (2015) 2971–2990, https://doi.org/10.3390/rs70302971.
[13] G. Messina, J.M. Peña, M. Vizzari, G. Modica, A comparison of UAV and satellites multispectral imagery in monitoring onion crop. An application in the 'Cipolla Rossa di Tropea' (Italy), Remote. Sens. 12 (20) (2020) 3424, https://doi.org/10.3390/rs12203424.
[14] J. Furlanetto, N. Dal Ferro, M. Longo, L. Sartori, R. Polese, D. Caceffo, L. Nicoli, F Morari, LAI estimation through remotely sensed NDVI following hail defoliation in maize (Zea mays L.) using Sentinel-2 and UAV imagery, Precision Agric. 24 (4) (2023) 1355–1379, https://doi.org/10.1007/s11119-023-09993-9.
[15] L. Pastonchi, S.F. Di Gennaro, P. Toscano, A. Matese, Comparison between satellite and ground data with UAV-based information to analyse vineyard spatio-temporal variability: This article is published in cooperation with the XIIIth International Terroir Congress November 17-18 2020, Adelaide, Australia. Guests editors: Cassandra Collins and Roberta De Bei, OENO One 54 (4) (2020) 919–934, https://doi.org/10.20870/oeno-one.2020.54.4.4028.
[16] N. Bollas, E. Kokinou, V. Polychronos, Comparison of Sentinel-2 and UAV multispectral data for use in precision agriculture: an application from Northern Greece, Drones 5 (2) (2021) 35, https://doi.org/10.3390/drones5020035.
[17] S.F. Di Gennaro, R. Dainelli, A. Palliotti, P. Toscano, A. Matese, Sentinel-2 validation for spatial variability assessment in overhead trellis system viticulture versus UAV and agronomic data, Remote. Sens. 11 (21) (2019) 2573, https://doi.org/10.3390/rs11212573.
[18] A. Rejeb, A. Abdollahi, K. Rejeb, H. Treiblmaier, Drones in agriculture: a review and bibliometric analysis, Comput. Electron. Agric. 198 (2022) 107017, https://doi.org/10.1016/j.compag.2022.107017.
[19] R. Martínez-Peña, S. Vélez, R. Vacas, H. Martín, S. Álvarez, Remote sensing for sustainable pistachio cultivation and improved quality traits evaluation through thermal and Non-Thermal UAV vegetation Indices, Appl. Sci. 13 (13) (2023) 7716, https://doi.org/10.3390/app13137716.
[20] J. Théau, E. Gavelle, P. Ménard, Crop scouting using UAV imagery: a case study for potatoes, J. Unmanned Vehicle Syst. 8 (2) (2020) 99–118, https://doi.org/10.1139/juvs-2019-0009.
[21] C. Ju, J. Kim, J. Seol, H.I. Son, A review on multirobot systems in agriculture, Comput. Electron. Agric. 202 (2022) 107336, https://doi.org/10.1016/j.compag.2022.107336.
[22] E. Yaacoub, M.-S. Alouini, A Key 6G challenge and opportunity—Connecting the base of the pyramid: a survey on rural connectivity, Proc. IEEE 108 (4) (2020) 533–582, https://doi.org/10.1109/JPROC.2020.2976703.
[23] Wang Sun, Lu Ding, Sun, Remote measurement of apple orchard canopy information using unmanned aerial vehicle photogrammetry, Agronomy 9 (11) (2019) 774, https://doi.org/10.3390/agronomy9110774.
[24] C. Zhang, J. Valente, W. Wang, L. Guo, A. Tubau Comas, P. Van Dalfsen, B. Rijk, L. Kooistra, Feasibility assessment of tree-level flower intensity quantification from UAV RGB imagery: a triennial study in an apple orchard, ISPRS J. Photogramm. Remote Sens. 197 (2023) 256–273, https://doi.org/10.1016/j.isprsjprs.2023.02.003.
[25] G. Jang, J. Kim, J.-K. Yu, H.-J. Kim, Y. Kim, D.-W. Kim, K.-H. Kim, C.W. Lee, Y. S. Chung, Review: cost-effective unmanned aerial vehicle (UAV) Platform for field plant breeding application, Remote. Sens. 12 (6) (2020) 998, https://doi.org/10.3390/rs12060998.
[26] E. Seifert, S. Seifert, H. Vogt, D. Drew, J. Van Aardt, A. Kunneke, T. Seifert, Influence of drone altitude, image overlap, and optical sensor resolution on multi-view reconstruction of forest images, Remote. Sens. 11 (10) (2019) 1252, https://doi.org/10.3390/rs11101252.
[27] M. García-Fernández, E. Sanz-Ablanedo, J.R. Rodríguez-Pérez, High-resolution drone-acquired RGB imagery to estimate spatial grape quality variability, Agronomy 11 (4) (2021) 655, https://doi.org/10.3390/agronomy11040655.
[28] A.L.A. Ribeiro, G.M. Maciel, A.C.S. Siquieroli, J.M.Q. Luz, R.B.D.A. Gallis, P.H.D. S. Assis, H.C.R.M. Catão, R.Y. Yada, Vegetation indices for predicting the growth and harvest rate of lettuce, Agriculture 13 (5) (2023) 1091, https://doi.org/10.3390/agriculture13051091.
[29] A. Agapiou, Vegetation extraction using visible-bands from openly licensed unmanned aerial vehicle imagery, Drones 4 (2) (2020) 27, https://doi.org/10.3390/drones4020027.
[30] J. Bendig, K. Yu, H. Aasen, A. Bolten, S. Bennertz, J. Broscheit, M.L. Gnyp, G. Bareth, Combining UAV-based plant height from crop surface models, visible, and near infrared vegetation indices for biomass monitoring in barley, Int. J. Appl. Earth Obs. Geoinf. 39 (2015) 79–87, https://doi.org/10.1016/j.jag.2015.02.012.
[31] H. Cen, L. Wan, J. Zhu, Y. Li, X. Li, Y. Zhu, H. Weng, W. Wu, W. Yin, C. Xu, Y. Bao, L. Feng, J. Shou, Y. He, Dynamic monitoring of biomass of rice under different nitrogen treatments using a lightweight UAV with dual image-frame snapshot

cameras, Plant Methods 15 (1) (2019) 32, https://doi.org/10.1186/s13007-019-0418-8.
[32] C.J. Tucker, Red and photographic infrared linear combinations for monitoring vegetation, Remote Sens. Environ. 8 (2) (1979) 127–150, https://doi.org/10.1016/0034-4257(79)90013-0.
[33] M. Louhaichi, M.M. Borman, D.E. Johnson, Spatially located platform and aerial photography for documentation of grazing impacts on wheat, Geocarto International 16 (1) (2001) 65–70, https://doi.org/10.1080/10106040108542184.
[34] A.A. Gitelson, Y.J. Kaufman, R. Stark, D. Rundquist, Novel algorithms for remote estimation of vegetation fraction, Remote Sens. Environ. 80 (1) (2002) 76–87, https://doi.org/10.1016/S0034-4257(01)00289-9.
[35] P.A. Burrough, R. McDonnell, C.D. Lloyd, Principles of Geographical Information Systems, Third edition, Oxford University Press, 2015.
[36] D. Shepard, A two-dimensional interpolation function for irregularly-spaced data, in: *Proceedings of the 1968 23rd ACM National Conference On* -, 1968, pp. 517–524, https://doi.org/10.1145/800186.810616.
[37] T. Hengl, A Practical Guide to Geostatistical Mapping, Office for Official Publications of the European Communities, 2009.
[38] A. Baddeley, E. Rubak, R. Turner, Spatial Point patterns: Methodology and Applications With R, CRC Press, 2016.
[39] Franklin, W.R. (1973). *Triangulated irregular network program*.
[40] J. Gallier, Geometric Methods and Applications: For Computer Science and Engineering, 38, Springer, New York, 2011, https://doi.org/10.1007/978-1-4419-9961-0.
[41] J. Lee, Comparison of existing methods for building triangular irregular network, models of terrain from grid digital elevation models, Int. J. Geograph. Inf. Syst. 5 (3) (1991) 267–285, https://doi.org/10.1080/02693799108927855.
[42] P. Mao, J. Ding, B. Jiang, L. Qin, G.Y. Qiu, How can UAV bridge the gap between ground and satellite observations for quantifying the biomass of desert shrub community? ISPRS J. Photogramm. Remote Sens. 192 (2022) 361–376, https://doi.org/10.1016/j.isprsjprs.2022.08.021.
[43] S.S. Choudhary, S. Biswal, R. Saha, C. Chatterjee, A non-destructive approach for assessment of nitrogen status of wheat crop using unmanned aerial vehicle equipped with RGB camera, Arabian J. Geosci. 14 (17) (2021) 1739, https://doi.org/10.1007/s12517-021-08139-3.
[44] B. Song, K. Park, Detection of aquatic plants using multispectral UAV imagery and vegetation index, Remote. Sens. 12 (3) (2020) 387, https://doi.org/10.3390/rs12030387.
[45] C. Pañitrur-De la Fuente, H. Valdés-Gómez, J. Roudet, N. Verdugo-Vásquez, Y. Mirabal, V.F. Laurie, J.P. Goutouly, C. Acevedo Opazo, M. Fermaud, Vigor thresholded NDVI is a key early risk indicator of Botrytis bunch rot in vineyards, OENO One 54 (2) (2020) 279–297, https://doi.org/10.20870/oeno-one.2020.54.2.2954.
[46] S. Vélez, M. Ariza-Sentís, J. Valente, Mapping the spatial variability of Botrytis bunch rot risk in vineyards using UAV multispectral imagery, Eur. J. Agron. 142 (2023) 126691, https://doi.org/10.1016/j.eja.2022.126691.
[47] M.F. Lopresti, C.M. Di Bella, A.J. Degioanni, Relationship between MODIS-NDVI data and wheat yield: a case study in Northern Buenos aires province, Argentina, Inf. Process. Agric. 2 (2) (2015) 73–84, https://doi.org/10.1016/j.inpa.2015.06.001.
[48] L. Sun, F. Gao, M. Anderson, W. Kustas, M. Alsina, L. Sanchez, B. Sams, L. McKee, W. Dulaney, W. White, J. Alfieri, J. Prueger, F. Melton, K. Post, Daily mapping of 30 m LAI and NDVI for grape yield prediction in california vineyards, Remote. Sens. 9 (4) (2017) 317, https://doi.org/10.3390/rs9040317.
[49] S. Vélez, J.A. Rubio, M.I. Andrés, E. Barajas, Agronomic classification between vineyards ('Verdejo') using NDVI and Sentinel-2 and evaluation of their wines, VITIS - J. Grapevine Res. (2019) 33–38, https://doi.org/10.5073/VITIS.2019.58.SPECIAL-ISSUE.33-38.
[50] S. Vélez, Potential of functional analysis applied to Sentinel-2 time-series to assess relevant agronomic parameters at the within-field level in viticulture, Comput. Electron. Agric. 11 (2022).
[51] R.E. White, Understanding Vineyard Soils, Second edition, Oxford University Press, 2015.
[52] X.-D. Yang, J. Wang, M.-S. Xu, A. Ali, Y. Xu, D. Lamb, L.-C. Duan, K.-H. Yan, S.-T. Yang, Effects of the ephemeral stream on plant species diversity and distribution in an alluvial fan of arid desert region: an application of a low altitude UAV, PLoS One 14 (2) (2019) e0212057, https://doi.org/10.1371/journal.pone.0212057.
[53] S. Fountas, E. Anastasiou, A. Balafoutis, S. Koundouras, S. Theoharis, N. Theodorou, The influence of vine variety and vineyard management on the effectiveness of canopy sensors to predict winegrape yield and quality, in: International Conference of Agricultura Engineering, Zurich, 2014.
[54] I. Sa, M. Popović, R. Khanna, Z. Chen, P. Lottes, F. Liebisch, J. Nieto, C. Stachniss, A. Walter, R. Siegwart, WeedMap: a large-scale semantic weed mapping framework using aerial multispectral imaging and deep neural network for precision farming, Remote. Sens. 10 (9) (2018) 1423, https://doi.org/10.3390/rs10091423.
[55] D. Ledderhof, R. Brown, A. Reynolds, M. Jollineau, Using remote sensing to understand Pinot noir vineyard variability in Ontario, Can. J. Plant Sci. 96 (1) (2016) 89–108, https://doi.org/10.1139/cjps-2015-0120.
[56] S. Vélez, E. Barajas, J.A. Rubio, R. Vacas, C. Poblete-Echeverría, Effect of missing vines on total leaf area determined by NDVI calculated from sentinel satellite data: progressive vine removal experiments, Appl. Sci. 10 (10) (2020) 3612, https://doi.org/10.3390/app10103612.
[57] M. Habib, Y. Alzubi, A. Malkawi, M. Awwad, Impact of interpolation techniques on the accuracy of large-scale digital elevation model, Open Geosciences 12 (1) (2020) 190–202, https://doi.org/10.1515/geo-2020-0012.
[58] R.D. Ward, N.G. Burnside, C.B. Joyce, K. Sepp, The use of medium point density LiDAR elevation data to determine plant community types in Baltic coastal wetlands, Ecol. Indic. 33 (2013) 96–104, https://doi.org/10.1016/j.ecolind.2012.08.016.
[59] L. Klerkx, E. Jakku, P. Labarthe, A review of social science on digital agriculture, smart farming and agriculture 4.0: New contributions and a future research agenda, NJAS: Wageningen J. Life Sci. 90–91 (1) (2019) 1–16, https://doi.org/10.1016/j.njas.2019.100315.
[60] A. Eltner, G. Sofia, Structure from motion photogrammetric technique. Developments in Earth Surface Processes, Elsevier, 2020, pp. 1–24, https://doi.org/10.1016/B978-0-444-64177-9.00001-1. Vol. 23.
[61] S. Openshaw, The Modifiable Areal Unit Problem, Geo Books, 1984.
[62] D.E. Jelinski, J. Wu, The modifiable areal unit problem and implications for landscape ecology, Landscape Ecol. 11 (3) (1996) 129–140, https://doi.org/10.1007/BF02447512.
[63] F. Lu, Y. Sun, F. Hou, Using UAV visible images to estimate the soil moisture of steppe, Water 12 (9) (2020) 2334, https://doi.org/10.3390/w12092334.
[64] T. Angelopoulou, N. Tziolas, A. Balafoutis, G. Zalidis, D. Bochtis, Remote sensing techniques for soil organic carbon estimation: a review, Remote. Sens. 11 (6) (2019) 676, https://doi.org/10.3390/rs11060676.
[65] T. Gorji, A. Tanik, E. Sertel, Soil salinity prediction, monitoring and mapping using modern technologies, Procedia Earth Planet. Sci. 15 (2015) 507–512, https://doi.org/10.1016/j.proeps.2015.08.062.
[66] M. Ladoni, H.A. Bahrami, S.K. Alavipanah, A.A. Norouzi, Estimating soil organic carbon from soil reflectance: A review, Precision Agric. 11 (1) (2010) 82–99, https://doi.org/10.1007/s11119-009-9123-3.
[67] R. Gerhards, D. Andújar Sanchez, P. Hamouz, G.G. Peteinatos, S. Christensen, C Fernandez-Quintanilla, Advances in site-specific weed management in agriculture—A review, Weed Res. 62 (2) (2022) 123–133, https://doi.org/10.1111/wre.12526.
[68] S. Vélez, C. Poblete-Echeverría, J.A. Rubio, R. Vacas, E. Barajas, Estimation of Leaf Area Index in vineyards by analysing projected shadows using UAV imagery, OENO One 55 (4) (2021) 159–180, https://doi.org/10.20870/oeno-one.2021.55.4.4639.
[69] A.I. Pavlova, Analysis of elevation interpolation methods for creating digital elevation models, Optoelectronics, Instrum. Data Process. 53 (2) (2017) 171–177, https://doi.org/10.3103/S8756699017020108.
[70] M. Ariza-Sentís, S. Vélez, R. Martínez-Peña, H. Baja, J. Valente, Object detection and tracking in precision farming: a systematic review, Comput. Electron. Agric. 219 (2024) 108757, https://doi.org/10.1016/j.compag.2024.108757.
[71] G. Farjon, L. Huijun, Y. Edan, Deep-learning-based counting methods, datasets, and applications in agriculture: a review, Precision Agric. (2023), https://doi.org/10.1007/s11119-023-10034-8.